Solution and Solid-State Structure of 2- and 4-Bis(trimethylsilyl)methylpyridinium Cations

Kathyrn Hassall, Carl H. Schiesser, and Jonathan M. White*

School of Chemistry and the BIO-21 Institute, The University of Melbourne, Victoria 3010, Australia

Received January 17, 2007

N-Methylation of the 2- and 4-bis(trimethylsilyl)methyl pyridines **7** and **9** gives the ions **5** and **6** and results in a significant decrease in the $^{13}CH-^{29}SiMe_3$ coupling constant, consistent with increased C−Si−π hyperconjugation between the trimethylsilyl substituents and the electron-deficient aromatic system of the pyridinium cations. The rotation barrier about the $C_{ipso}-CH$ bond, which was measured for both **5** and **7** using variable-temperature ^{13}C NMR and calculated at the B3LYP/6-311G** level, reveals that steric effects make a larger contribution than hyperconjugative effects to this barrier. The crystal structure of the protonated salt **11** shows that the conformation of the $CH(SiMe_3)_2$ substituent is similar to that predicted by calculations and allows for both $C-SiMe_3$ bonds to interact with the aromatic π-system.

Introduction

The structural effects of C−Si hyperconjugation have been demonstrated in a number of systems, ranging from substituted benzenes with low electron demand[1,2] to tropylium cations[3] and vinyl cations.[4] We have found that trialkylsilylmethyl-substituted pyridinium cations provide a convenient system for investigating C−Si hyperconjugation in cationic systems with relatively low electron demand. These crystalline cations are relatively stable to desilylation, and structural and spectroscopic information can be obtained.[5,6] For example both the 2- and 4-substituted trialkylsilylmethyl-substituted *N*-methyl pyridinium ions **1** and **2** have been investigated in both the solid state and solution.[6] In the solid state X-ray analysis reveals that C−Si hyperconjugation in **1** and **2** manifests in lengthening of the CH_2-Si bond distance and shortening of the $CH_2-C(Ar)$ bond distance, reflecting contributions of the double-bond-no-bond resonance forms **1′** and **2′** to the ground-state structures of these ions.

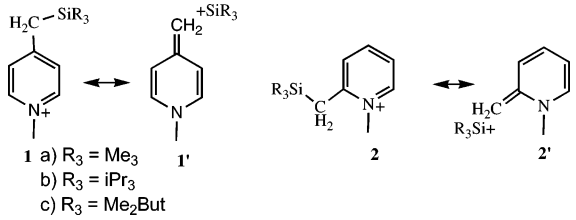

1 a) $R_3 = Me_3$ **1'**
b) $R_3 = iPr_3$
c) $R_3 = Me_2But$

2 **2'**

These ions have also been investigated in solution using ^{13}C and ^{29}Si spectroscopy. C−Si−π hyperconjugation reveals itself as a downfield shift in the ^{29}Si chemical shift and a decrease in the $^{29}Si-^{13}C$ coupling constant upon methylation of the precursor pyridine derivatives **3** and **4**. Both effects are larger in magnitude for the 2-substituted derivatives,[6] in qualitative agreement with calculations.[7]

Scheme 1

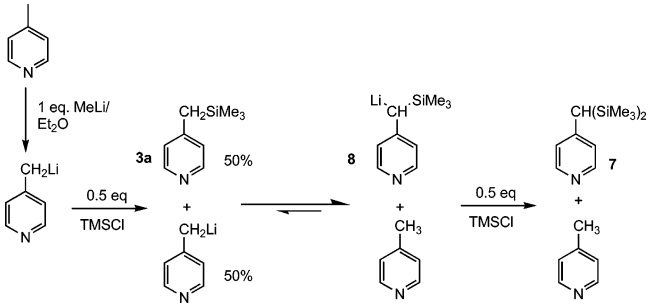

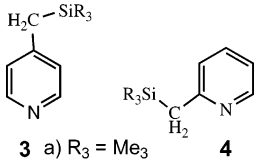

3 a) $R_3 = Me_3$ **4**
b) $R_3 = iPr_3$
c) $R_3 = Me_2But$

We were interested in determining the structures and properties of the doubly silylated system **5** and **6**. These ions were interesting because geometrical constraints may result in differing degrees of hyperconjugation of the two trimethylsilyl substituents with the aromatic π-system, which may be reflected in differing structural parameters for these substituents.

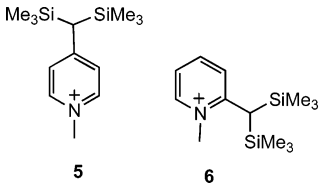

5 **6**

Results and Discussion

The precursor to **5**, 4-bis(trimethylsilyl)methylpyridine (**7**), was prepared in a one-step reaction from 4-picoline (Scheme

* Corresponding author. E-mail: whitejm@unimelb.edu.au.

(1) Lambert, J. B.; Singer, R. A. *J. Am. Chem. Soc*. **1992**, *114*, 10246.
(2) Lambert, J. B.; Shawl, C. E.; Basso, E. *Can. J. Chem*. **2000**, *78*, 1441.
(3) Hassall, K.; White, J. M. *Org. Lett.* **2004**, *6*, 1737.
(4) Müller, T.; Juhasz, M.; Reed, C. A. *Angew. Chem., Int. Ed.* **2004**
(5) Happer, A.; Ng, J.; Pool, B.; White, J. *J. Organomet. Chem.* **2002**, *659*, 10.
(6) Hassall, K.; Lobachevsky, S.; White, J. M. *J. Org. Chem*. **2005**, *70*, 1993.
(7) Hassall, K.; Lobachevsky, S.; White, J. M.; Schiesser, C. H. *Organometallics* **2007**, in press.

10.1021/om070045+ CCC: $37.00
Publication on Web 05/18/2007

Table 1. One-Bond Coupling Constants and ^{29}Si NMR Chemical Shifts for 1−7 and 9[c]

cmpd	CH_2−Si	Si−C(R)	δ ^{29}Si	cmpd	CH_2−Si	Si−C(R)	δ ^{29}Si	ΔJ (Hz)[d]
1a	35.9	52.7	12.8	**3a**	41.8	51.9	6.9	−5.9
1b	35.0	52.6	15.5	**3b**	40.4	52.6	6.3	−5.4
1c	35.0[b]	51.9	16.8	**3c**	41.9	51.2	8.8	−6.9[b]
2a[a]	35.0	52.6		**4a**	43.5	52.1	7.2	−8.5
2b	32.8	53.4	17.03	**4b**	41.2	51.9	6.7	−8.4
2c	33.0	51.9	18.5	**4c**	42.7	51.1	9.1	−9.7
5	36.6	52.6	9.3	**7**	41.2	52.0	2.1	−4.6
6	34.5	51.8	12.2	**9**	41.2	52.6	2.2	−6.7

[a] The ^{29}Si δ value for **2a** could not be reliably determined due to slow desilylation during data acquisition. [b] The ^{13}C−^{29}Si coupling constant for **1c** could not be reliably determined due to the overlap of ^{13}C peaks. [c] The data for **1**−**4** are reported in ref 2. [d] This is the change in the Si−CH_2 coupling constant upon methylation.

1), which was lithiated at room temperature with 1.05 equiv of methyl lithium in diethyl ether, then quenched slowly with 1 equiv of trimethylsilyl chloride. Using this method the predominant product was the bis-substituted pyridine **7** compared to the monosubstituted derivative **3a** when the lithiated solution is inversely added to the chlorosilane as per White et al.[5] The formation of **7** is rationalized by the increased acidity of the methylene protons in Ar−CH_2SiMe_3 compared to Ar−CH_3.[8] As a result, **3a**, formed upon addition of trimethylsilyl chloride, is lithiated *in situ* by 4-lithiomethylpyridine, resulting in formation of **7** (via **8**) in 70% yield, based on trimethylsilyl chloride. In addition to the recovery of picoline a small percentage of **1a** (<10%) can be isolated. The pyridine precursor (**9**) to ion **6** was prepared in a similar way from 2-picoline.

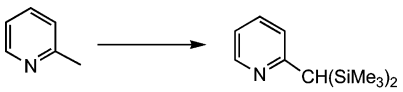

9

Methylation of **7** and **9** with methyl triflate in deuteroacetonitrile resulted in **5** and **6** as their triflate salts, which were stable for weeks at room temperature. The ^{13}C NMR spectrum was consistent with clean formation of the products. The ^{13}C−^{29}Si one-bond coupling constants and ^{29}Si NMR chemical shifts for **5** and **6** and the previously reported monosilylated derivatives **1a**−**4a** for comparison are reported in Table 1.

Similarly to the monosubstituted series **1**−**4** reported previously,[6] a greater change in both the ^{13}C−^{29}Si one-bond coupling constants and ^{29}Si NMR chemical shifts occurred upon methylation of the 2-substituted derivative **6** compared to the 4-position of **5**. However, in both cases at room temperature, the two silyl substituents were equivalent by ^{13}C and ^{29}Si NMR, suggesting rapid interconversion between the various degenerate conformations on the NMR time scale. Compared to the monotrimethylsilylmethyl pyridines, **3a** and **4a**, the change in ^{13}C−^{29}Si one-bond coupling constants upon methylation is less in magnitude for the bis-substituted **5** and **6**. This is expected, as the effects of hyperconjugation would be diluted over the two silicon substituents.

Attempts to obtain crystals of **5** were unsuccessful. Although NMR revealed methylation of **7** was successfully achieved in solution using methyl iodide, methyl tosylate, or methyl triflate, both the triflate and iodide salts of **5** formed oils. Crystals were obtained from the tosylate derivative of **5**; however these proved to be *N*-methyl-4-methylpyridinium, **10**, arising from desilylation during the crystallization, a process that we have observed with similar species previously.[6]

Fortunately protonation of **5**, with picric acid, in methanol, Scheme 2, followed by slow evaporation at room temperature resulted in X-ray quality crystals of 4-bis(trimethylsilyl)-

Scheme 2

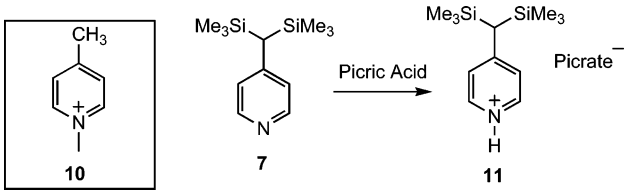

Table 2. Crystal Data and Refinement Details for 11·picrate

empirical formula	$C_{18}H_{26}N_4O_7Si_2$
fw	466.61
temperature	130(2) K
wavelength	0.71073 Å
crystal syst	triclinic
space group	$P\bar{1}$
unit cell dimens	a = 8.1984(11) Å, α = 69.703(3)°
	b = 12.0862(17) Å, β = 82.395(2)°
	c = 12.4671(17) Å, γ = 80.066(3)°
volume	1137.7(3) Å^3
Z	2
density (calcd)	1.362 mg/m^3
absorp coeff	0.202 mm^{-1}
F(000)	492
cryst size	0.40 × 0.30 × 0.10 mm^3
θ range for data collection	1.75 to 24.99°
index ranges	$-9 \le h \le 9$, $-14 \le k \le 13$,
	$-13 \le l \le 14$
no. of reflns collected	6030
no. of indep reflns	3946 [R(int) = 0.0380]
completeness to θ = 24.99°	98.7%
refinement method	full-matrix least-squares on F^2
no. of data/restraints/params	3946/0/290
goodness-of-fit on F^2	0.898
final R indices [$I > 2\sigma(I)$]	R_1 = 0.0423, wR_2 = 0.0805
R indices (all data)	R_1 = 0.0589, wR_2 = 0.0848
largest diff peak and hole	0.343 and −0.269 e Å^{-3}

Table 3. Selected Bond Distances (Å) and Angles (deg) for 11·picrate

bond length		bond length		bond angle	
N1−C1	1.336(3)	C3−C6	1.491(3)	Si1−C6−C3	117.2
C1−C2	1.373(3)	C6−Si1	1.912(2)	Si2−C6−C3	114.6
C2−C3	1.403(3)	C6−Si2	1.907(2)	Si1−C6−Si2	117.2
C3−C4	1.396(3)	Si1−CH_3(av)	1.865	Si1−C6−C3−C2	−78.3
C4−C5	1.372(3)	Si2−CH_3(av)	1.867	Si1−C6−C3−C4	101.2
C5−N1	1.338(3)			Si2−C6−C3−C2	56.3
				Si2−C6−C3−C4	−124.20

methylpyridinium, **11**·picrate. Unfortunately, for the 2-substituted pyridine analogue **9**, crystallization of both the methylated and protonated derivatives gave only desilylated products.

Crystal data for **11**·picrate were measured at low temperature to minimize the unwanted effects of thermal motion. Crystal data and refinement details are presented in Table 2, selected bond distances, angles and dihedral angles are listed in Table 3, and a perspective diagram is presented in Figure 1.

The bond distances within the aromatic ring, which are related by the local plane of symmetry bisecting N1 and C3, agree well,

(8) Colvin, E. *Silicon in Organic Synthesis*; Butterworth: Boston, 1981.

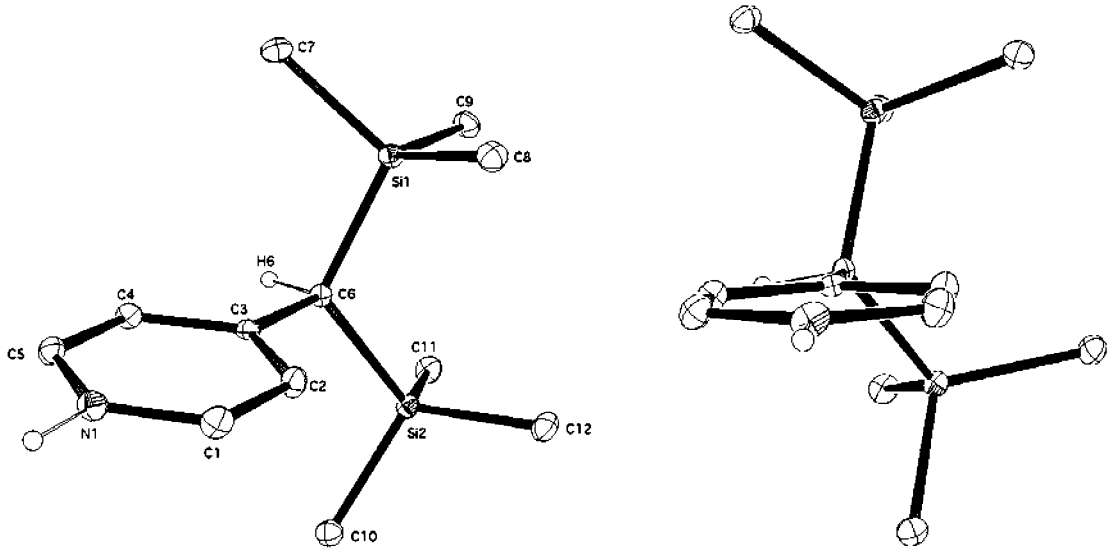

Figure 1. Thermal ellipsoid plot of **11**. Ellipsoids are shown at 20% probability. Labeled view, a, and view along the pyridinium plane showing off-center alignment of the C_6-Si_1 bond, b. Most hydrogens and the picrate counterion have been removed for clarity.

and the relative distances are consistent with contributions of resonance forms related to **1′**. The two Si−CH_2 bond distances are longer than standard values (1.878 Å),[5] consistent with the expected effects of hyperconjugation with the charged pyridinium ring, but do not differ significantly from one another. The conformation of the $CH(SiMe_3)_2$ substituent, as defined by the dihedral angles Si1−C6−C3−C2 and Si2−C6−C3−C4, shows that neither C−Si bond is perfectly coplanar with the π-system, but rather both deviate slightly, C6−Si1 by 11.5° and C6−Si2 by 34.0°, Figure 1 and Table 2. If we consider that the overlap between the C−Si bond and the pyridinium π-system is proportional to $\cos^2\theta$, where θ is the angle between the C−Si bond and the π-system,[9] then hyperconjugation of one of the C−Si bonds and the π-system is quite close to optimal while the other is slightly less so. As such, it is not surprising that (i) both C−Si bond distances are longer than standard values and (ii) there is little difference between them.

Since there are two silicon substituents present in **11**, the degree of hyperconjugation can be estimated by the sum of $\cos^2(\theta_1) + \cos^2(\theta_2)$, where θ_1 and θ_2 are the Si−CH_2−C(ipso)−C(ortho) dihedral angles. In a simple tetrahedral atom the angle, in projection, between two substituents is 120°. In this example the X-ray structure shows the two trimethylsilyl groups are pushed away from an idealized tetrahedral value of 109.5° to 117.2°, presumably to relieve steric interactions. The angle that the two silicons make (when projected in the Si1/Si2/H6 plane) was calculated by three-dimensional trigonometry to be 134.8°; as such, $\theta_2 = 134.8 + \theta_1$ (see Figure 1). This was used to plot $\cos^2(\theta_1) + \cos^2(\theta_2)$ over varying θ_1 from 0° to 180°.

This simple calculation shows that hyperconjugation is maximized when $\theta_1 = 20°$, not $\theta_1 = 0°$, where one silicon is preferentially aligned coplanar to the π-system. This is depicted in Figure 3b, where both silicons participate in hyperconjugation to varying degrees. The X-ray crystal structure, which showed an 11.5° off-center alignment of the C−Si1 bond, is consistent with these results, and this point is indicated in Figure 2. This point is slightly less than the optimum calculated angle; however steric effects will also affect this result. These results are

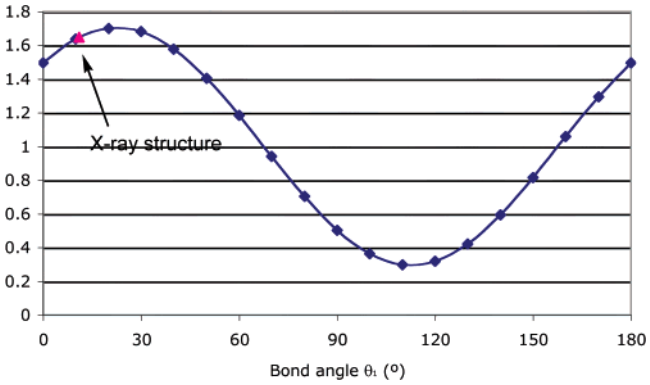

Figure 2. Graph showing how $\sum(C-Si-\pi)$ hyperconjugation varies with dihedral angle. The degree of hyperconjugation is measured by $\cos^2(\theta_1) + \cos^2(134.8 + \theta_1)$.

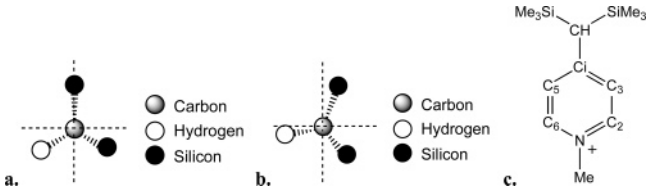

Figure 3. Pictorial representation of the alignment of the C−H and C−Si bonds along the C3−C6 bond: (a) $\theta_1 = 0°$ and (b) $\theta_1 = 20°$. (c) Labeled diagram of **5**.

supported by those calculated by Siehl[10] for a disilyl-substituted vinyl cation. In this example the most stable conformation resulted in both Si−C bonds lying 30° off coplanar alignment.

Examination of Figure 2 illustrates that the rotation of the $C_i-CH(SiMe_3)_2$ group occurs at the expense of hyperconjugation. It is this rotation that allows for the C3 and C5 carbons to be equivalent on the NMR time scale. The barrier to rotation about the $C_i-CH(SiMe_3)_2$ will have a hyperconjugative component and a steric component. Therefore we decided to measure the barrier to rotation by variable-temperature NMR. In fact at room temperature broadening of the peak corresponding to C3/C5 of **5** was observed. A variable-temperature ^{13}C NMR

(9) Radom, L.; Hehre, W. J.; Pople, J. A. *J. Am. Chem. Soc.* **1972**, *92*, 2371. Rappoport, Z.; Abramovitch, B.; Karni, M.; Apeloig, Y. *Isr. J. Chem.* **1989**, *29*, 267.

(10) Siehl, H.-U.; Kaufmann, F.-P.; Apeloig, Y.; Braude, V.; Danovitch, D.; Berndt, A.; Stamatis, N. *Angew. Chem., Int. Ed.* **1991**, *30*, 1479.

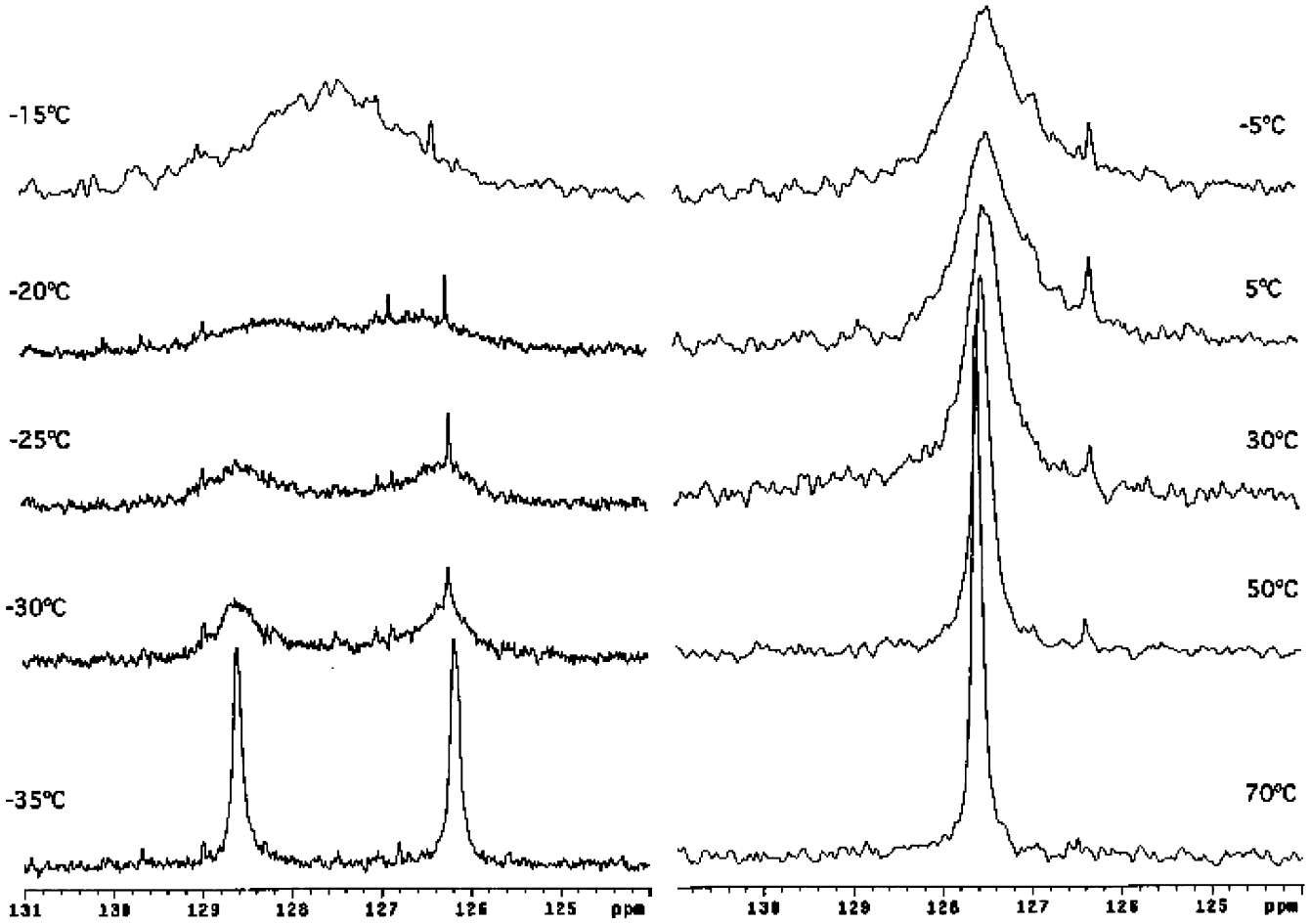

Figure 4. ^{13}C NMR spectrum (131−124 ppm) for 5·triflate, −35 to +70 °C.

experiment was run (Figure 4). At −35 °C two independent signals are observed for C3 and C5, while at +70 °C a single sharp signal is observed for both carbons. These results are consistent with a fixed geometry of both silicon substituents at low temperature, which would remove the symmetry from the pyridinium ring.

The ^{13}C NMR of the nonmethylated precursor, **7**, also showed slight broadening of the C3/C5 peak at room temperature. This was also analyzed by variable-temperature NMR in the same solvent as **5**·triflate, deuteroacetonitrile. This could only be measured as low as −40 °C, before freezing of the solvent prevented further measurements. At this point 1 equiv of deuterodichloromethane was added to the solution to allow for the acquisition of lower temperature spectra. The spectrum at −40 °C was reacquired with the "mixed" solvent, and this was compared to the "single" deuteroacetonitrile solvent only. The degree of line broadening was found to be quite similar in both solvents. The mixed solvent was then used for low-temperature acquisitions (−40 to −65 °C) and compared directly to the deuteroacetonitrile acquisitions (from −30 to +20 °C), Figure 5.

From the variable-temperature NMR analysis the energy of the rotation barrier for the bis(trimethylsilyl)methyl group can be estimated. The ^{13}C NMR spectrum was simulated using the WINDNMR software,[11] and the barrier for rotation was estimated as 49.2 ± 1.1 kJ/mol for the methylated derivative, **5**. This was compared to the nonmethylated pyridine precursor, **7**, where the degree of hyperconjugation should be substantially reduced, and a barrier of 47.3 ± 1.1 kJ/mol was obtained. The small difference between the two indicates that steric effects, rather than hyperconjugative effects, are the major contributor to the rotation barrier in these derivatives.

The pyridine precursor, **7**, and the methylated pyridinium cation, **5** (Figure 6) were modeled by *ab initio* (RHF/3-21G(*)) and density functional (B3LYP/6-311G**) methods using Gaussian 03.[12] For **5** and **7** the optimal geometries were calculated at the lower level, without restriction (*E*(min)). The Si1−C6−C4−C1 dihedral angle was then fixed at intervals of 15° over a 360° range, the geometry was optimized, and the energy was calculated at each point. The difference in energy (ΔE, where $\Delta E = E(\text{x}^\circ) - E(\text{min})$) was plotted against the dihedral angle in Figure 7.

The rotational transition state for **7**, pictorially represented in Figure 8, corresponds to the point at which the nonbonding

(11) Reich, H. J. *WINDNMR*; J. Chem. Educ. Software, 3D2: 1996.

(12) Frisch, M. J.; Trucks, G. W.; Schlegel, H. B.; Scuseria, G. E.; Robb, M. A.; Cheeseman, J. R.; Montgomery, J. A., Jr.; Vreven, T.; Kudin, K. N.; Burant, J. C.; Millam, J. M.; Iyengar, S. S.; Tomasi, J.; Barone, V.; Mennucci, B.: Cossi, M.; Scalmani, G.; Rega, N.; Petersson, G. A.; Nakatsuji, H.; Hada, M.; Ehara, M.; Toyota, K.; Fukuda, R.; Hasegawa, J.; Ishida, M.; Nakajima, T.; Honda, Y.; Kitao, O.; Nakai, H.; Klene, M.; Li, X.; Knox, J. E.; Hratchian, H. P.; Cross, J. B.; Adamo, C.; Jaramillo, J.; Gomperts, R.; Stratmann, R. E.; Yazyev, O.; Austin, A. J.; Cammi, R.; Pomelli, C.; Ochterski, J. W.; Ayala, P. Y.; Morokuma, K.; Voth, G. A.; Salvador, P.; Dannenberg, J. J.; Zakrzewski, V. G.; Dapprich, S.; Daniels, A. D.; Strain, M. C.; Farkas, O.; Malick, D. K.; Rabuck, A. D.; Raghavachari, K.; Foresman, J. B.; Ortiz, J. V.; Cui, Q.; Baboul, A. G.; Clifford, S.; Cioslowski, J.; Stefanov, B. B.; Liu, G.; Liashenko, A.; Piskorz, P.; Komaromi, I.; Martin, R. L.; Fox, D. J.; Keith, T.; Al-Laham, M. A.; Peng, C. Y.; Nanayakkara, A.; Challacombe, M.; Gill, P. M. W.; Johnson, B.; Chen, W.; Wong, M. W.; Gonzalez, C.; Pople, J. A. *Gaussian 03*, Revision B.05; Gaussian, Inc.: Pittsburgh, PA, 2003.

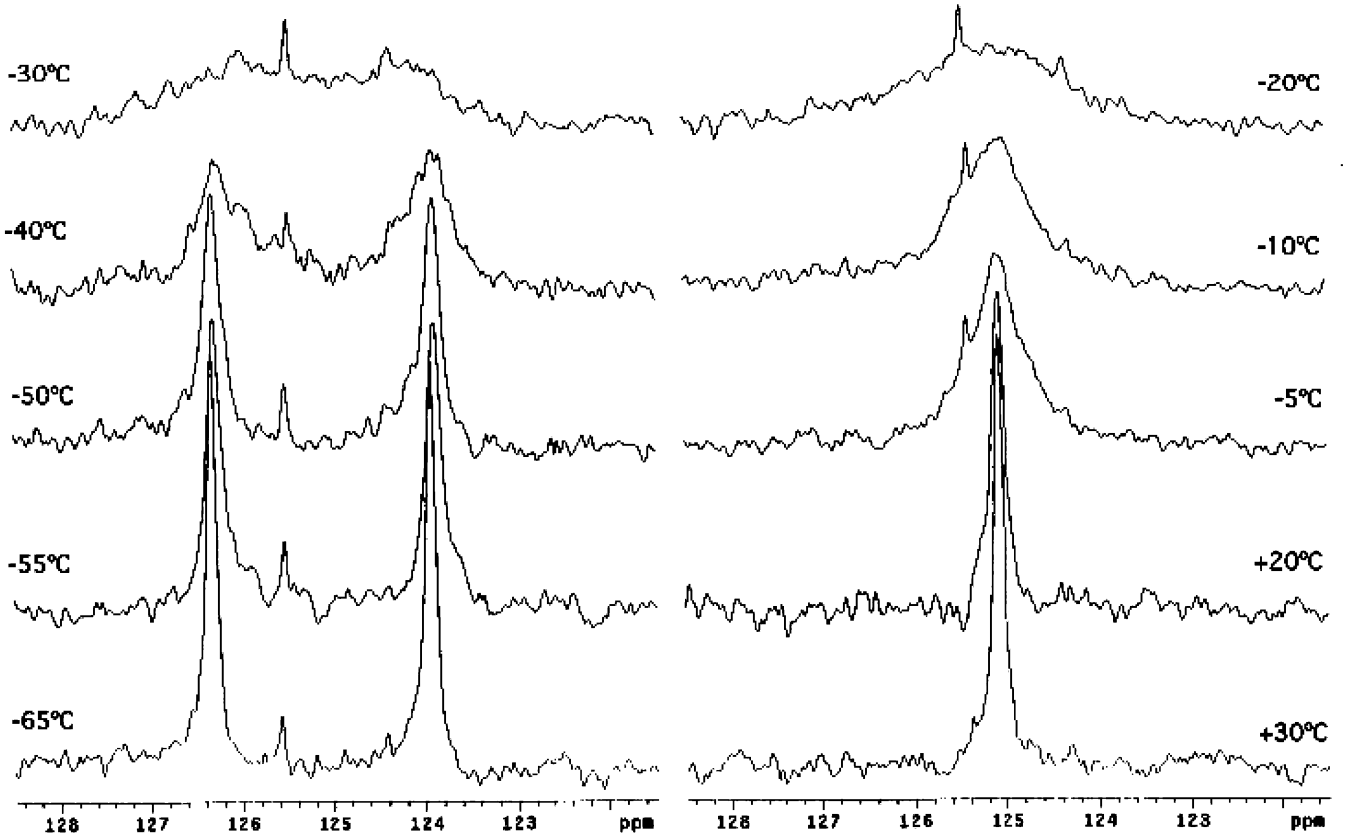

Figure 5. ^{13}C NMR spectrum (128.5−121.5 ppm) for **7**, −65 to +30 °C. Spectra for −65, −55, −50, −40, and +30 °C were recorded in 1:1 CD_3CN/CD_2Cl_2.

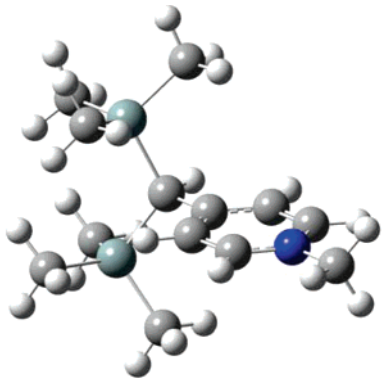

Figure 6. Optimized geometry of **5**, modeled at B3LYP/6-311G-(d,p).

repulsion between both silicon atoms and the pyridine ring is maximized. At this point the C−Si bond lengths, C6−Si2 and C6−Si1, are lengthened to 1.941 and 1.932 Å (RHF/3-21G-(*)), respectively. Bond angle distortions are unable to relieve the steric interaction between the substituent and the ortho carbons of the ring. At this point hyperconjugation will also be minimized.

The geometry at the second minimum is similar to that of the overall minimum. Steric interactions of the silicon substituents are relieved by distortion of the C6−C_{ipso}−C_{ortho} bond angle, which is 120.9° on the hydrogen side and 122.3° on the silicon side. This distortion places the hydrogen closer and silicon further away from the pyridine ring. Hyperconjugative interaction at this geometry is also close to maximum. Similar geometries were observed for **5** at the minimum and maximum.

Since the energy arising from steric effects should be the similar for the two species **5** and **7**, the difference in energy

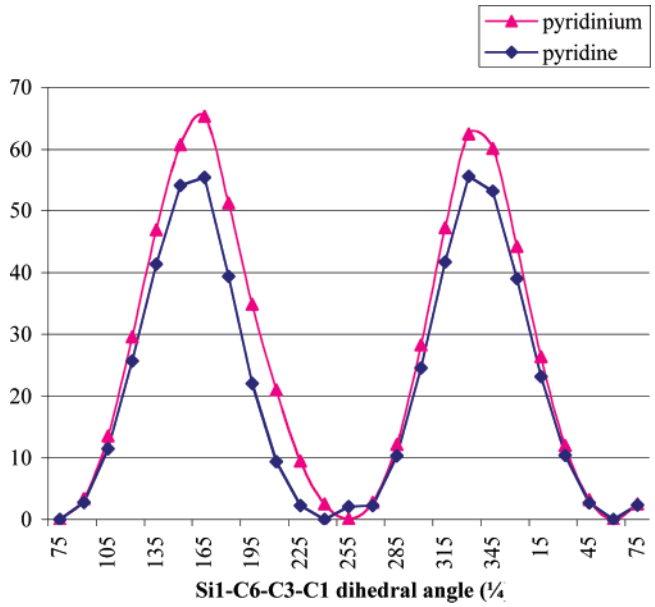

Figure 7. Plot showing how ΔE (kJ/mol) varies with the Si1−C6−C3−C1 dihedral angle (deg), where $\Delta E = E(x°) - E(\text{min})$.

between the ΔE_{max}(pyridinium **7**) and the ΔE_{max}(pyridine **5**) is an estimation of the difference in hyperconjugation between the two species. The value predicted by these low-level calculations is somewhat larger than that obtained by variable-temperature NMR; however the relative magnitudes of the hyperconjugative and steric components of the rotation barrier are in qualitative agreement.

The ground-state (∼75°) and rotational transition-state (∼170°) structures for **5** and **7** were further optimized at the B3LYP/6-

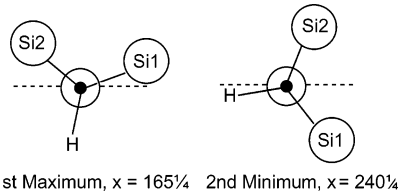

Figure 8. Pictorial representation of geometries at first maximum and second minimum for **5**. The plane of the pyridine ring is represented by the dashed line.

311G** level of theory using standard gradient techniques and the optimized structures verified as corresponding to local minima and saddle points, respectively, by frequency analysis. These calculations predict rotational energy barriers of 51.7 and 58.7 kJ/mol for **7** and **5**, respectively. The small calculated difference of some 7 kJ/mol compares favorably with those obtained from the NMR study (*vide supra*).

Conclusion

A significant decrease in the $^{13}C-^{29}Si$ coupling constants in the pyridinium ions **5** and **6** compared to their pyridine precursors **7** and **9** is consistent with increased $C-Si-\pi$ hyperconjugation between the trimethylsilyl substituents and the electron-deficient aromatic system of the pyridinium cation. However the increased hyperconjugation has only a small effect on the barrier for rotation about the $C_{ipso}-CH(SiMe_3)_2$, suggesting that this barrier is mainly determined by steric effects; this is in qualitative agreement with calculations. In the crystal structure of the protonated pyridine **11** as its picrate salt, the conformation of the $CH(SiMe_3)_2$ substituent is similar to that predicted by calculations and allows for both $C-SiMe_3$ bonds to interact with the aromatic π-system.

Experimental Section

X-ray Crystallography. Crystals of **11**·picrate were grown from methanol. The temperature during data collection was maintained at 130.0(1) K using an Oxford Cryostream cooling device. Intensity data were collected with a Bruker SMART Apex CCD detector using Mo Kα radiation (graphite crystal monochromator λ = 0.71073). Data were reduced using the program SAINT.[13]

The structure was solved by direct methods and difference Fourier synthesis. Thermal ellipsoid plots were generated using the program ORTEP-3[14] integrated within the WINGX[15] suite of programs

Synthesis. General experimental details are published elsewhere.[6]

4-Bis(trimethylsilyl)methylpyridine, 7. Methyl lithium (1.4 M in hexane, 20 mL, 28.0 mmol) was added to a solution of 4-picoline (2.5 mL, 2.35 g, 25.3 mmol) in ether (15 mL) and refluxed for 30 min. The solution was allowed to cool to room temperature, and a solution of trimethylsilyl chloride (3.45 g, 32.0 mmol) in ether (5 mL) was added dropwise over 30 min. After the addition was complete the solution was stirred for an additional 1 h before quenching with water (30 mL). The organic layer was washed with water (2 × 30 mL), then purified via acid/base extraction to afford a yellow oil. Further purification was achieved by dry-flash column chromatography (ethyl acetate/hexane) (2.65 g, 70%)

^{1}H NMR: (400 MHz, $CDCl_3$) δ 8.32 (2H, d, J = 6.4 Hz, H2/6), 6.84 (2H, d, J = 6.0 Hz, H3/5), 1.55 (1H, s, CH), 0.01 (18H, s, $Si-CH_3$). ^{13}C NMR: (100 MHz, $CDCl_3$) δ 153.8 (C4), 148.7 (C2/6), 124.2 (C3/5), 30.7 (CH, $^1J_{C-Si}$ = 41.2 Hz), −0.03 ($Si-CH_3$, $^1J_{C-Si}$ = 52.0 Hz). ^{29}Si NMR: (80 MHz, $CDCl_3$) δ 2.13. ESI-MS (*m/z*): 208.1 (M + 1).

***N*-Methyl 4-Bis(trimethylsilyl)methylpyridinium Triflate, 5.** A solution of **77** (100 mg) in deuteroacetonitrile (0.5 mL) was treated with neat methyl triflate (1.05 equiv).

^{1}H NMR: (400 MHz, CD_3CN) δ 8.35 (2H, d, J = 7.2 Hz, H2/6), 7.48 (2H, d, J = 6.8 Hz, H3/5), 4.16 (3H, s, $N-CH_3$), 2.35 (1H, s, CH), 0.09 (18H, s, $Si-CH_3$). ^{13}C NMR: δ (100 MHz, CD_3CN) δ 167.8 (C4), 144.5 (C2/6), 127.4 (C3/5), 121.4 (CF_3, J = 319 Hz), 47.6 ($N-CH_3$), 35.3 (CH, $^1J_{C-Si}$ = 36.6 Hz), 0.01 ($Si-CH_3$, $^1J_{C-Si}$ = 52.6 Hz). ^{29}Si NMR: (80 MHz, CD_3CN) δ 9.27.

2-Bistrimethylsilylmethylpyridine, 9. To an ice-cooled solution of *n*-butyl lithium (1.6 M, 10 mL, 16 mmol) and TMEDA (2.36 mL, 13.5 mmol) under N_2 atmosphere was slowly added 2-picoline (1.25 mL, 13.5 mmol), resulting in an orange solution. Trimethylsilylmethyl chloride (1.71 mL, 14.6 mmol) was added slowly over 30 min, resulting in a yellow solution, which became colorless after stirring overnight. The product was purified by acid/base extraction to afford a clear oil (0.531 g, 31%).

^{1}H NMR: (400 MHz, $CDCl_3$) δ 8.31 (1H, dd, J = 5.2, 1.5 Hz, H6), 7.37 (1H, ddd, J = 7.6, 7.6, 1.5 Hz, H4), 6.82 (2H, m, H3/5), 1.85 (1H, s, CH), −0.02 (18H, s, $SiMe_3$). ^{13}C NMR: (100 MHz, $CDCl_3$) δ 163.8 (*C*2), 148.6 (C6), 135.3 (C4), 122.5 (C3), 118.2 (C5), 33.0 (CH, $^1J_{C-Si}$ = 41.2 Hz), −0.05 ($SiMe_3$, $^1J_{C-Si}$ = 51.8 Hz). ^{29}Si NMR: (80 MHz, $CDCl_3$) δ 2.21.

***N*-Methyl 2-Bistrimethylsilylmethylpyridinium Triflate, 6.** A solution of **81** (100 mg) in deuteroacetonitrile (0.5 mL) was treated with neat methyl triflate (1.05 equiv).

^{1}H NMR: (400 MHz, CD_3CN) δ 8.55 (1H, d, J = 5.7 Hz, H6), 8.27 (1H, ddd, J = 7.7, 7.7, 1.4 Hz, H4), 7.61−7.56 (2H, m, H3/5), 4.13 (3H, s, $N-CH_3$), 2.64 (1H, s, CH), 0.13 (18H, s, $SiMe_3$). ^{13}C NMR: (100 MHz, CD_3CN) δ 163.8, 147.5, 145.0, 128.7, 123.2, 47.8 (N−Me), 30.0 (CH, $^1J_{C-Si}$ = 34.5 Hz), 0.21 ($Si-CH_3$, $^1J_{C-Si}$ = 52.6 Hz). ^{29}Si NMR: (80 MHz, CD_3CN) δ 12.21.

Crystallographic data supplied in CIF format have been deposited with the Cambridge Crystallographic Data Centre, CCDC reference numbers 646234.

Acknowledgment. Ours thanks go to the University of Melbourne MRDGS scheme for financial support and to Australian Research Council for the award of an APRA (K.H.) and the Victorian Institute for Chemical Sciences High Performance Computing Facility.

Supporting Information Available: A full listing of geometries and energies (Gaussian Archive entries) of structures studied is provided. This material is available free of charge via the Internet at http://pubs.acs.org.

OM070045+

(13) Siemens. *SMART*, *SAINT*, *SADABS*; Siemens Analytical X-ray Instruments Inc.: Madison, WI, 1999.
(14) Farrugia, L. J. *J. Appl. Crystallogr.* **1997**, *30*, 565.
(15) Farrugia, L. J. *J. Appl. Crystallogr.* **1999**, *32*, 837.